ORIGINAL PAPER

Numerical investigation of mucociliary clearance using power law and thixotropic mucus layers under discrete and continuous cilia motion

M. A. Modaresi[1]

Abstract

Mucus layer movement inside the airway system is an important phenomenon as the first defensive mechanism against pathogens. This research deals with the mucus velocity variations inside the nasal cavity using two different power law and thixotropic mucus layers. The cilia movement is replaced with four cyclic velocity profiles at the lower boundary of the mucus layer, while the upper boundary is exposed to the free-slip condition. The effects of boundary conditions and different fluid parameters are evaluated on the mucus flow. Furthermore, the replacement of power law and thixotropic mucus layers with a high viscous Newtonian mucus is examined under the free-slip condition at the mucus upper boundary. The adaptation rate is used as the criteria for replacing fluids instead of each other. The results show the mucus flow has enough time to adjust the changes from the lower boundary and the recovery stroke does not affect the mucus velocity in the effective stroke. Moreover, it is observed that the mucus flow variations are the same under the influence of recovery, breakdown, and breakdown exponent parameters. However, the effects of the exponent parameter on the mucus flow are more than the other two parameters in the recovery stroke. It is concluded that the assumption for replacing the power law mucus with a high viscous Newtonian one is acceptable. However, this assumption leads to the maximum error of 98.5% for thixotropic mucus in the recovery stroke.

Keywords Mucociliary clearance · Mucus layer · Power law · Thixotropic · Cyclic conditions · Numerical simulation

1 Introduction

Evaluating the functionality of mucus flow is important as the first defensive mechanism against pathogens and viruses (Xu and Jiang 2019). Trapping and transferring harmful particles toward the stomach using the mucus flow is the so-called mucociliary clearance phenomenon (MCC) (Shang et al. 2019). Investigation of different aspects of MCC process has led to extensive researches including experimental inspections (Xu and Jiang 2019; Shang et al. 2019; Chen et al. 2018; Lubkin et al. 2007; Sedaghat et al. 2016a; Smith et al. 2008; Vasquez et al. 2016; Quraishi et al. 1998), mathematical models (Guo, et al. 1708; Cortez et al. 2005; Eloy and Lauga 2012; Osterman and Vilfan 2011; Gueron and

Liron 1992), and numerical simulations (Chen et al. 2018; Sedaghat et al. 2016a; Chatelin et al. 2017).

Exploring modern therapy methods encountered severe challenges in remedying airway diseases due to mucus flow (Quraishi et al. 1998). The limitation of measurement devices, continuous production of mucins through goblet cells, and the effects of boundary conditions on the mucus flow make the issue more complicated. Some experimental investigations addressed the effects of boundary conditions on the mucus flow in human bronchial epithelial (HBE) cell cultures using a rotational cylinder (Vasquez et al. 2016). The others investigated transferring viscoelastic and Newtonian mucus by cilia beating in cell cultures (Lubkin et al. 2007; Dillon et al. 2007; Mitran 2007; Sedaghat et al. 2016b; Lee et al. 2011).

The rate of MCC was specified by the Saccharin test (Shang et al. 2019). The saccharin test was a standard method where a saccharin particle was located 1 cm behind the anterior end of the inferior turbinate and the time was taken until the patient comprehended a sweet taste from the

✉ M. A. Modaresi
m.modaresi@modares.ac.ir

1 Department of Mechanical Engineering, Tarbiat Modares University, PO Box 14115-143, Tehran, Iran

saccharin. Moreover, the variation of MCC rate against diseases including cystic fibrosis caused difficulties in local therapy of nasal airway diseases (Derichs et al. 2011). Cystic fibrosis was one of the most widely recognized genetic diseases (Farrell 2008) which increased and decreased the mucus accumulation and surface liquid volume inside the nasal respiratory system, respectively (Derichs et al. 2011). MCC was in a high order of dependency with cilia beating frequency (Xu and Jiang 2019; Shang et al. 2019; Sedaghat et al. 2016a; Gizurarson 2015). Therefore, an evaluation of the effects of cilia movement on mucus flow was performed to develop multilayer models for MCC rate (Snyder et al. 1988; Hollenberg 1986).

Inspired by biological explorations, the development of different mathematical models was performed to understand the details of the underlying mechanisms of MCC process (Fauci and Dillon 2006; Lauga and Powers 2009). Mathematical models were developed to determine the formation of metachronal waves (rhythmic back-and-forth movement), conditions for the stability of the metachronal wave, the cilium mechanism to generate force for propelling the mucus, and the efficiency of MCC. The simple mathematical models were developed by studying the wavelike motion in polychaete worm (Gray 1939) and sea-urchin spermatozoa (Gueron and Liron 1992; Gray and Hancock 1955). These studies neglected the effects of fluid flow on cilia motion. The further models were established based on resistance theory (Xu and Jiang 2019) which considered the effects of fluid flow in modeling cilia (Eloy and Lauga 2012; Osterman and Vilfan 2011; Blake 1972, 1971; Barton and Raynor 1967). The metachronal wave led to a movement of the mucus layer with an average velocity of 5 mm min^{-1} (Illum 2003; Mistry et al. 2009). Therefore, to consider the effects of mucus flow on the cilia motion the inertia terms were neglected and the Navier–Stokes equations turned to Stokes equations. In this way, the Stokeslet method which was developed based on the slender body theory (Dusenbery 2009) used to solve the equations.

By using mathematical models, a variety of numerical investigations were conducted in different categories. The cilia beating frequency, the interaction between mucus flow and cilia, and the interaction between the airway surface liquid (ASL) layer and macroscale were different aspects of numerical simulations (Shang et al. 2019; Chen et al. 2018; Sedaghat et al. 2016a, b). The effects of cilia beating frequency were evaluated on MCC rate by Sedaghat et al. (Sedaghat et al. 2016a). The linear relation between MCC and cilia beating frequency was obtained as the result. Furthermore, the porosity effects on viscoelastic cilia-driven flow in a divergent channel were evaluated by Javid et al. (Javid et al. 2021), numerically. They analyzed 2D cilia-driven flow under different physical parameters and observed boundary layer phenomena in the velocity profile by increasing porosity and relaxation time. Moreover, increasing the porosity and viscoelastic effects led to the reduction of trapped bolus magnitude in the divergent channel. The effects of heat transfer and induced magnetic field were also inspected on the cilia-driven flow analytically by Ishtiaq et al. (Ishtiaq et al. 2022). It was concluded the velocity and magnetic fields were in opposite directions than the eccentricity parameter of the cilia equations. Furthermore, the temperature profile was increased for Prandtl and Eckert number, while it was decreased due to thermal radiation. The development of multilayer models for MCC was reviewed in another line of studies based on the interaction between mucus flow and cilia beating frequency (Shang et al. 2019; Sedaghat et al. 2016b). Moreover, the effects of different nasal cavities on the rate of MCC were inspected by many researchers (Gizurarson 2015; Pires et al. 2009; Corbo et al. 1989). It was concluded simulation of mucus flow inside 3D shell surface models provided a closer rate of MCC against experimental data (Shang et al. 2019).

Modeling the ASL layer as a single or two-layer model was one of the differences between numerical simulations. Based on the hypotonic-defensin hypothesis, the ASL layer was a single layer (Shang et al. 2019; Vasquez et al. 2016; King et al. 1993; Satir and Sleigh 1990; Sleigh 1977), while the modern hypothesis stated that it was a two-layer model (Sedaghat et al. 2016a, b; Ross and Corrsin 1974; Matar et al. 2002; Zhu 2019). The other difference was related to the boundary condition at the lower boundary of the ASL layer. The common boundary conditions were constant
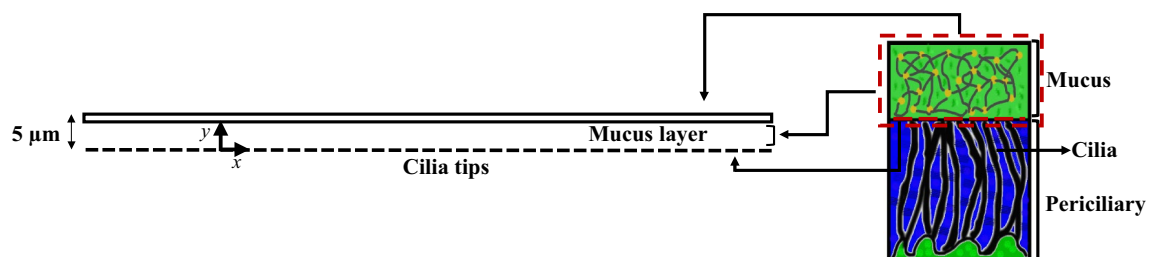

Fig. 1 Modeling of MCC structure inside the nasal cavity with two infinite parallel plates

(Shang et al. 2019) and continuous cyclic (sine or cosine) (Sedaghat et al. 2016a, b) velocities. However, the real boundary condition was neither constant nor continuous cyclic and should be applied at the mucus–periciliary interface (Vasquez et al. 2016). The last difference was the use of different fluids as mucus including viscoelastic (Sedaghat et al. 2016a, b; Vasquez et al. 2016), power law (Chatelin et al. 2017), and Newtonian fluids (Shang et al. 2019; Vasquez et al. 2016). On the other hand, the use of the free-slip condition at the upper boundary of the mucus layer was a common feature of numerical simulations.

Nowadays, the dangers of COVID-19 epidemic are plaguing most researchers all over the world to find different methods to prevent the penetration of viruses into the respiratory system (Zanin et al. 2016; Khashkhosha and Elhadi 2020; Sundararaman 2020; Chowdhury 2020). The impacts of COVID-19 on the respiratory system were discussed by Chowdhury et al. (Chowdhury 2020). Since the first defensive shield of the body against pathogens is the ASL layer (Sundararaman 2020), obtaining adequate knowledge is essential about the structure of the ASL layer under the influence of different conditions.

In the present study, two types of non-Newtonian fluids including power law and thixotropic are considered as the nasal mucus. Although the existence of cilia is neglected, their motion is replaced with four velocity profiles at the lower boundary of the mucus layer. The cyclic boundary conditions are continuous constant effective stroke, discrete constant effective and recovery strokes, continuous cyclic effective stroke, and discrete cyclic effective stroke along with constant recovery stroke. Moreover, the upper boundary of the mucus layer is exposed to free shear stress. The squared part in Fig. 1 is modeled using two infinite parallel plates to simulate mucus flow inside the nasal cavity.

2 Governing equations

The fluid flow is evaluated by the sets of continuity and momentum equations along with an extra constitutive equation related to the shear stress as follows:

$$\nabla . \mathbf{u} = 0 \tag{1}$$

$$\rho \left(\frac{\partial \mathbf{u}}{\partial t} + \mathbf{u} . \nabla \mathbf{u} \right) = \nabla . \boldsymbol{\sigma} \tag{2}$$

where $\mathbf{u}$, t, ρ, and $\boldsymbol{\sigma}$ are the velocity vector, time, density, and the Cauchy stress tensor, respectively. The Cauchy stress tensor is calculated by:

$$\boldsymbol{\sigma} = -p\mathrm{I} + \boldsymbol{\tau} \tag{3}$$

where $\boldsymbol{\tau}$, $\mathbf{I}$, p denote the extra stress tensor, the unit tensor, and the pressure, respectively. In this study, two different types of fluids including power law and thixotropic are considered as the mucus layer. The deviatoric stress tensor can be expressed as:

$$\begin{cases} \boldsymbol{\tau} = \left(k\dot{\gamma}^{n-1} + \dfrac{\tau_0}{\dot{\gamma}} \right) \dot{\boldsymbol{\gamma}} & \text{if } \tau > \tau_0 \\ \dot{\gamma} = 0 & \text{if } \tau \le \tau_0 \end{cases} \tag{4}$$

where τ_0, n, k, and $\dot{\boldsymbol{\gamma}}$ are the yield stress, the power index, the consistency index, and the deformation rate tensor, respectively. Moreover, τ and $\dot{\gamma}$ are the magnitudes of $\boldsymbol{\tau}$ and $\dot{\boldsymbol{\gamma}}$, respectively. The yield stress is equal to zero for the power law fluid.

Thixotropic fluid deals with the microstructure of materials which evolves with the time of flowing. The evolution of microstructure is modeled by the definition of a structural parameter λ ranging from 0 to 1 (Bui and Ho 2020). The

Fig. 2 Different velocity profiles exert on the mucus–periciliary interface **a** continuous constant effective stroke, **b** discrete constant effective and recovery strokes, **c** continuous cyclic effective stroke, **d** discrete cyclic effective stroke along with constant recovery stroke
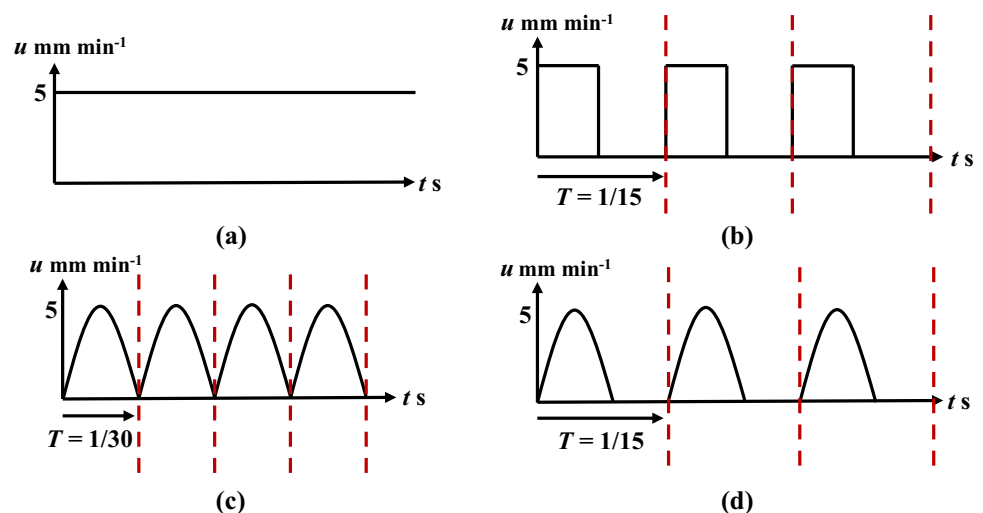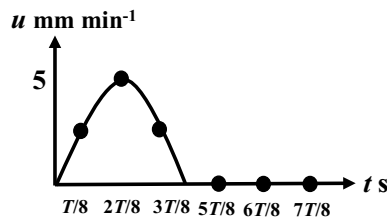
Fig. 3 Different flow times to examine velocity variations of the mucus layers

lower and upper limits correspond to completely broken and fully recovered states of the microstructure, respectively. The constitutive equation to calculate the rate of evolution for λ is determined by:

$$\frac{\partial \lambda}{\partial t} + \mathbf{u}.\nabla \lambda = K_1(1-\lambda)^m - K_2\lambda^n \tag{5}$$

where m and n are the rate indices and K_1 and K_2 are the rate parameters. The recovery and breakdown rates correspond to the first and second terms on the RHS of Eq. (5), respectively. In the present study, Burgos's (Burgos et al. 2001), thixotropic fluid is considered as the mucus layer with the following evolution equation for λ.

$$\frac{\partial \lambda}{\partial t} + \mathbf{u}.\nabla \lambda = \alpha(1-\lambda) - \beta_1 \lambda \dot{\gamma} \exp\left(\beta_2 \dot{\gamma}\right) \tag{6}$$

where α_1, β_1, and β_2 are the recovery, breakdown, and breakdown exponent parameters, respectively.

3 Physiology of the ASL layer

The polymeric structure of ASL consists of two different fluids (Sedaghat et al. 2016a; Quraishi et al. 1998): Newtonian and non-Newtonian (Quraishi et al. 1998). The Newtonian fluid (periciliary layer) is placed at the bottom of the non-Newtonian fluid (mucus) and provides one-way movement for the mucus layer (Blake 1971; Brennen 1974). The non-Newtonian mucus moves on the lower fluid by cilia beating which is the main mechanism for transporting pathogens and harmful substances (Blake 1971; Brennen 1974). Cilia beating is a composition of two different strokes: effective and recovery strokes (Xu and Jiang 2019). In the effective stroke, cilia penetrate the mucus layer and push it toward the esophagus (MCC) (Blake 1971; Brennen 1974) then detach from the mucus layer and move back through the periciliary layer in the recovery stroke. This type of cilia movement leads to unilateral movement of the mucus layer. Cilia are surrounded by the periciliary layer (Blake 1971, 1975; Brennen 1974; Brennen and Winet 1977) and perform rhythmic
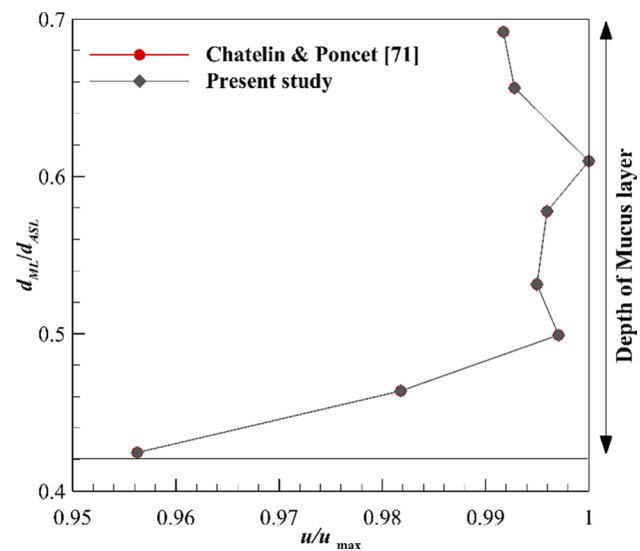

Fig. 4 Validation of numerical results against the available data (Chatelin and Poncet 2016)

back-and-forth movement (metachronal wave) (Blake 1971; Brennen 1974). The structure of the mucus layer is different in micro- and macroscales which behaves like a low viscous fluid and non-Newtonian one, respectively (Lai et al. 2009). Mucus constituents are 0.02% DNA, 1% lipids, 1% mineral, 2–3% glycoproteins and proteins, and 95% water (Potter et al. 1967; Matthews et al. 1963). The total height of mucus layers is 15 μm (Gizurarson 2015) which 33% is related to the thickness of the mucus layer (Shang et al. 2019), and the rest belongs to the periciliary layer (Quraishi et al. 1998). At the resting rate secretion of mucus is about 0.5–1 ml cm^{-2} mucus over 24 h which moves toward the posterior of the nasopharynx (Quraishi et al. 1998) with the rate of 5–10 mm min^{-1} (Illum 2003; Mistry et al. 2009; Lale et al. 1998; Rusznak et al. 1994). The rate of mucus flow is in a high order of dependency with the cilia beating frequency (Xu and Jiang 2019; Shang et al. 2019; Sedaghat et al. 2016a; Gizurarson 2015) and the evaluated frequencies are 15 Hz ($T = 1/15$ s) and 30 Hz ($T = 1/30$ s) in the present study (Cornaz and Buri 1994; Ugwoke et al. 2001; Sanderson and Sleigh 1981). The density of goblet cells specifies the mucus secretion which is about 5700–11,000 cells per ml (Dalhamn 1956) in adults. When the rate of mucus secretion exceeds the normal state (Rhinorrhea) (Myon et al. 2010), the mucus is directed out of the respiratory tract due to the disability of the cilia in transferring extra mucus. Furthermore, respiratory mucosa contains enzymes including lysozyme that play a key role in eliminating harmful particles (Singh et al. 2002).
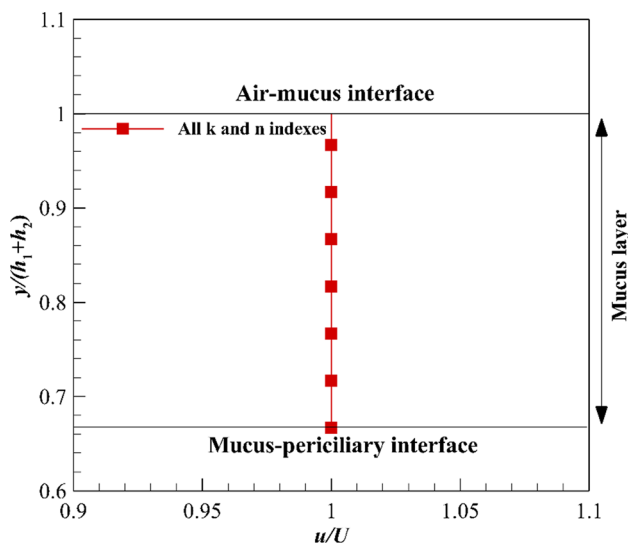
Fig. 5 Velocity variations of the mucus layer using profile (a) along with zero shear stress on the upper bound of the mucus layer for different power and consistency indexes
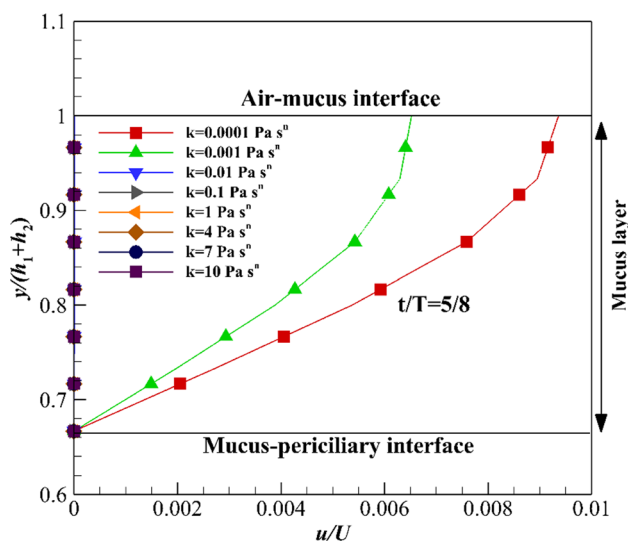

Fig. 6 Velocity variations of the mucus layer using profile (b) in the recovery stroke along with zero shear stress on the upper bound of the mucus layer for different consistency indexes with $n = 0.482$

4 Boundary conditions

Simulation of mucus flow is performed between two parallel plates with a length-to-the hydraulic diameter ratio (L/D_h) of 300. D_h is the hydraulic diameter and defined using Eq. (7).

$$D_h = 4A/P \tag{7}$$

where A and P are the flow cross section and wetted perimeter of the cross section, respectively (Kahramanoglu et al. 2017).

The applied boundary conditions to the computational domain are the free shear stress at the top of the mucus layer, atmospheric pressure at the outlet boundary, and different velocity profiles at the lower bound of the mucus layer. The different patterns of velocity profiles are exposed on the bottom plate shown in Fig. 2.

As the first step in mucus flow simulation, the assumption of permanent contact of cilia and the mucus layer (constant effective stroke) is investigated (profile (a)). By applying the recovery stroke to profile (a), the effects of both effective and recovery strokes are examined on the mucus layer variations (profile (b)).

In the second step, the effect of gradual effective stroke is evaluated by substituting profile (a) with profile (c). Furthermore, to consider a more realistic motion for cilia beating the combination of the gradual effective and recovery strokes is used for further numerical simulations (profile (d)). Figure 3 indicates different flow times to examine velocity variations of the mucus layer.

5 Numerical procedure

Incompressible and unsteady 2D Navier–Stokes equations are solved numerically to obtain variations of the mucus velocity field. Due to the high viscosity of the mucus layer and the cilia metachronal wave, the mucus movement is generally from the anterior to the posterior of the nasal cavity and there is nearly no lateral mucus movement (Xu and Jiang 2019; Gsell et al. 2020; Schneiter et al. 2021). Therefore, the mucus movement in the third direction is neglected. The high order of viscous forces against the inertia forces inside the mucus layer (Re $\ll$ 1) leads to discretize the convection terms with the central scheme. To accelerate the convergence rate of the solution, multi-grid method is applied to the equations. Furthermore, to handle the pressure–velocity coupling the PIMPLE algorithm (Roohi et al. 2016) is used and the flow variables are stored using the arrangement of a collocated grid (Round 1980; Flórez-Orrego et al. 2012). By setting the time step size to 10^{-5}, the courant number ($u\Delta t/\Delta x$) is controlled during the numerical solutions less than one. To obtain the convergence stability for the solution, the residuals of all variables are set to less than 10^{-9}. All numerical solutions are accomplished using OpenFOAM 7 packages.

The grid independency test and uncertainty of grid discretization are evaluated using the grid convergence index (GCI) (Celik et al. 2008). The grid size of 5×10^4 results in the GCI factor less than 2% for the velocity variations inside the mucus layer all over the computational domain.
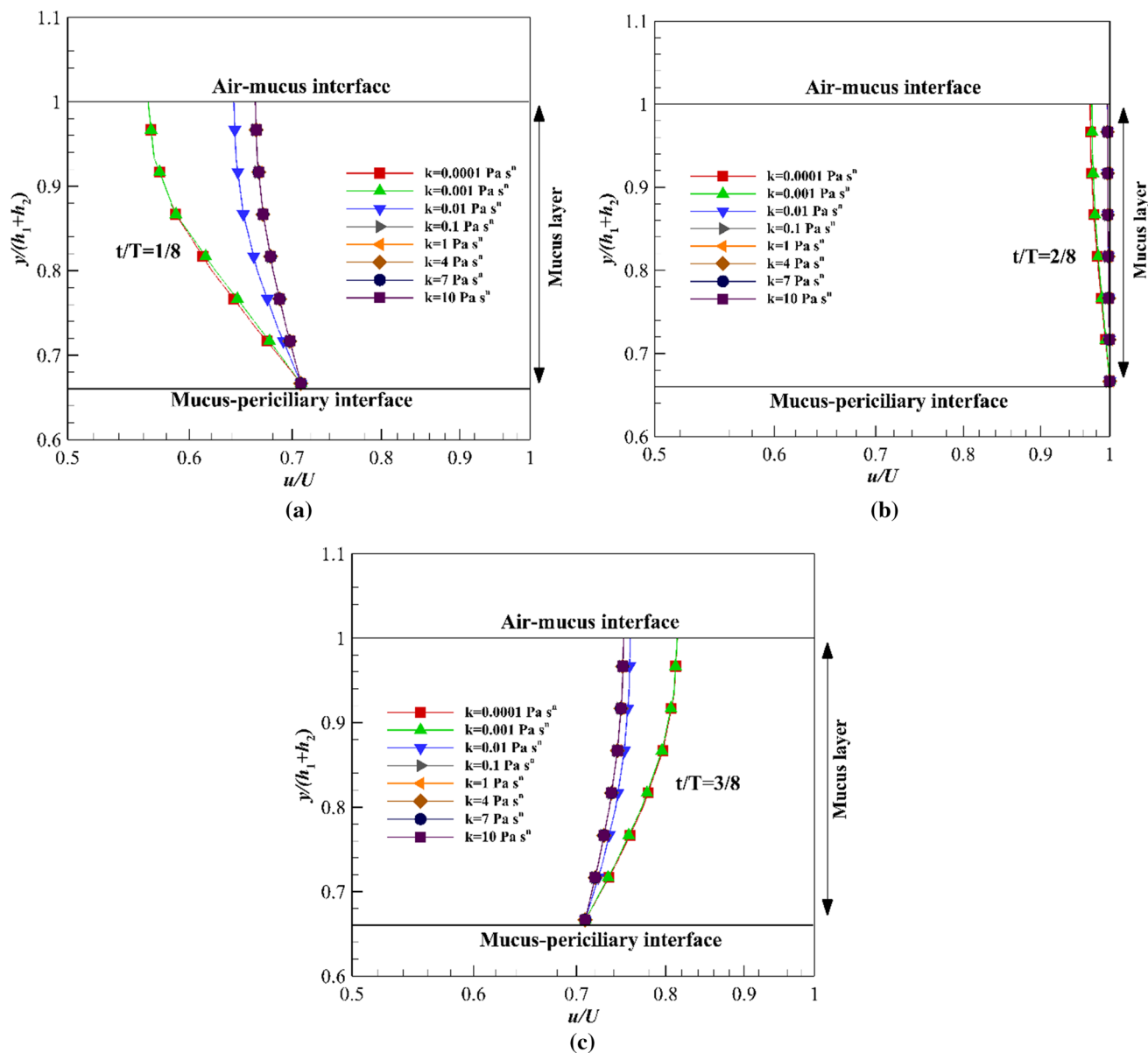
Fig. 7 Velocity variations of the mucus layer using profile (c) affected by zero shear stress on the upper bound of the mucus layer for different consistency indexes with $n = 0.482$ **a** $t/T = 1/8$, **b** $t/T = 2/8$, **c** $t/T = 3/8$

Table 1 Maximum adaptation rates for a range of consistency indexes using profile (c)

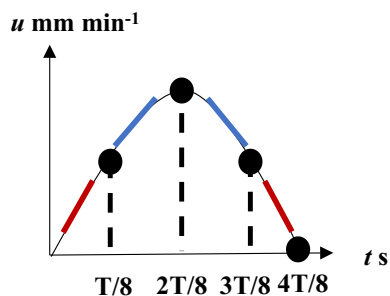| Times	Maximum adaptation rates for a range of consistency indexes (%)			
	$k = 0.0001$	$k = 0.001$	$k = 0.01$	$k \geq 0.01$
$t/T = 1/8$	79	79	90.4	93.4
$t/T = 2/8$	97	97.3	99.65	99.65
$t/T = 3/8$	85.2	85.2	93	94.4

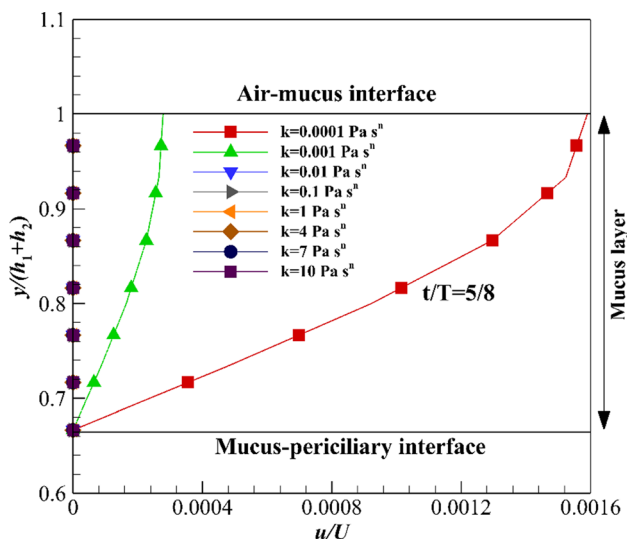**Fig. 8** Different acceleration and deceleration rates over time

Fig. 9 Velocity variations of the mucus layer using profile (d) in the recovery stroke along with zero shear stress on the upper bound of the mucus layer for different consistency indexes with $n = 0.482$
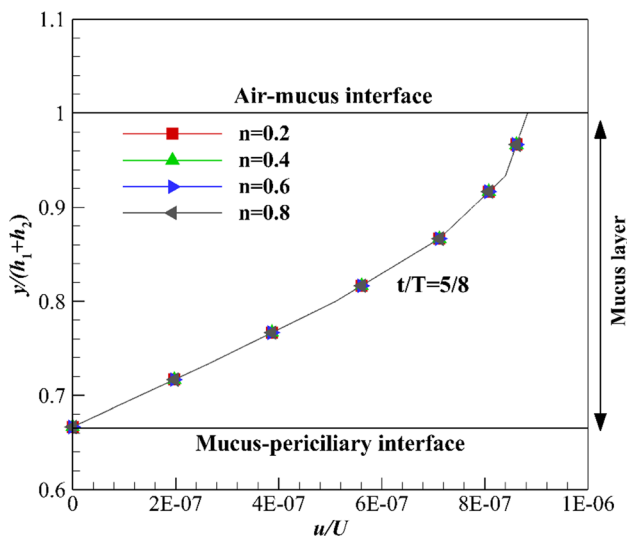

Fig. 10 Velocity variations of the mucus layer using profile (b) in the recovery stroke along with zero shear stress on the upper bound of the mucus layer for different power indexes with $k = 0.355$

6 Results and discussion

Velocity variations inside the mucus layer are discussed using two different approaches: power law and thixotropic in the following subsections. A variety of different boundary conditions are applied on the lower bound of the computational domain as cilia motion to evaluate the response of the mucus layer. Furthermore, the effects of different parameters including the power index, the consistency index, and the recovery and breakdown parameters on the behavior of the mucus layer are examined using two different fluids, separately. The duration of each simulation is 5 s equivalent to 150 and 75 cycles for cilia oscillating frequencies 30 and 15 Hz, respectively, and the results are extracted from the last cycle. Figure 4 shows the validation of numerical results against the available in Ref (Chatelin and Poncet 2016), and d_{ML} and d_{ASL} are the depth of mucus and ASL layers, respectively.

6.1 Power law mucus layer

The power index is less than one ($n < 1$) to save the shear-thinning property of the mucus layer. The effects of different power and consistency indexes are investigated separately. The power and consistency indexes are 0.482 and 0.355 for a healthy mucus layer, respectively (Chatelin et al. 2017). Therefore, all the numerical simulations are performed for the effects of different power and consistency indexes at $k = 0.355$ and $n = 0.482$, respectively.

Figure 5 indicates the velocity variation of the mucus layer affected by profile (a) for a range of power and consistency indexes ($n = 0.2$–0.8 and $k = 10^{-4}$–10). The constant effective stroke provides sufficient time for the mucus flow to adjust the changes from the bottom plate, and the mucus layer characteristics become independent of the changes in fluid indexes. Therefore, the velocity field all over the layer is the same as the velocity at the lower bound.

6.1.1 Influence of the consistency index (k)

By applying profile (b) to the lower bound of the mucus layer, the effects of different consistency indexes are determined on the mucus velocity field in the recovery stroke (Fig. 6). Increasing the consistency index leads to an increment of the adaptation rate of the mucus layer with the changes from the bottom plate. Adaptation rate describes the response rate of mucus layer velocity to the changes from the mucus–periciliary interface velocity. According to Fig. 6, variations of the mucus layer become independent of the changes in the consistency index for values greater than 0.01 ($k \geq 10^{-2}$). The changes in the mucus layer are consistent with the changes in the bottom plate and are independent of the fluid indexes when the constant effective stroke of profiles (a) and (b) is applied to the lower bound, because the mucus flow has enough time to respond to the changes from the bottom plate.

Substituting profile (a) with profile (c) (gradual effective stroke) provides transient variations for the mucus flow, and there is not enough time to adapt to the changes from the bottom plate. Figure 7 shows the mucus velocity at different times using profile (c). Although the adaptation rate increases with the increment of the consistency index, the
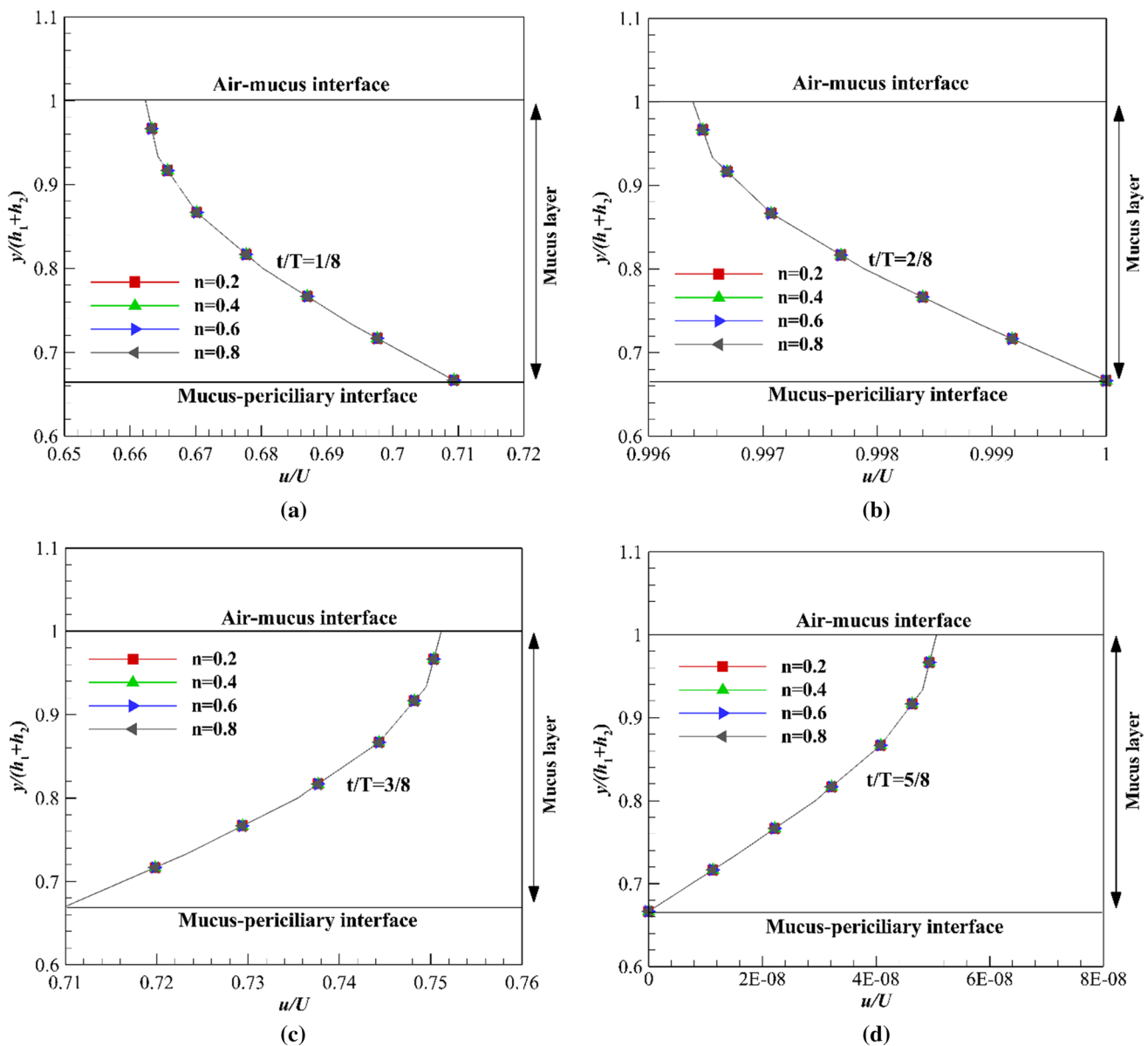
Fig. 11 Velocity variations of the mucus layer using profiles (c) and (d) affected by zero shear stress on the upper bound of the mucus layer for different power indexes with $k = 0.355$ **a** $t/T = 1/8$, **b** $t/T = 2/8$, **c** $t/T = 3/8$, **d** $t/T = 5/8$ (recovery stroke of profile (d))

Table 2 Maximum adaptation rates for a range of power indexes using profile (c)

Times	Maximum adaptation rates for a range of power indexes ($n = 0.2$–0.8) (%)
$t/T = 1/8$	93.2
$t/T = 2/8$	99.64
$t/T = 3/8$	94.1

$$\text{Adaptation rate} = 100 - \frac{\left| \left(\frac{u}{U}\right)_{\text{interface}} - \left(\frac{u}{U}\right)_{\text{mucus}} \right|}{\left(\frac{u}{U}\right)_{\text{interface}}} \times 100 \tag{8}$$

The differences between acceleration rates at periods ($t/T = 0$ to $t/T = 1/8$) and ($t/T = 1/8$ to $t/T = 2/8$) and deceleration rates at periods ($t/T = 2/8$ to $t/T = 3/8$) and ($t/T = 3/8$ to $t/T = 4/8$) cause differences between adaptation rates (Fig. 8). The rates of acceleration and deceleration at periods ($t/T = 0$ to $t/T = 1/8$) and ($t/T = 3/8$ to $t/T = 4/8$) are more than

rate of adaptation increases and decreases over time, repeatedly (Table 1). The maximum adaptation rate is taken into account using Eq. (8).
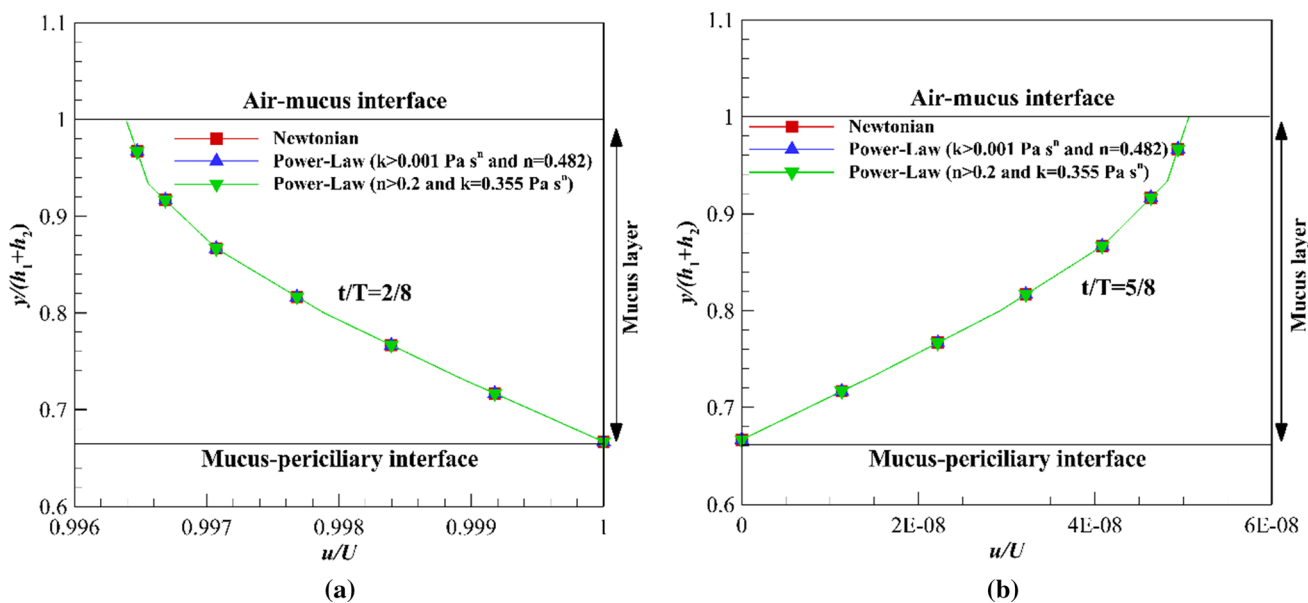
Fig. 12 Comparison of mucus layer velocity using both Newtonian and power law fluids affected by profile (d) and zero shear stress on the upper bound of the mucus layer for different power and consistency indexes **a** effective stroke, **b** recovery stroke
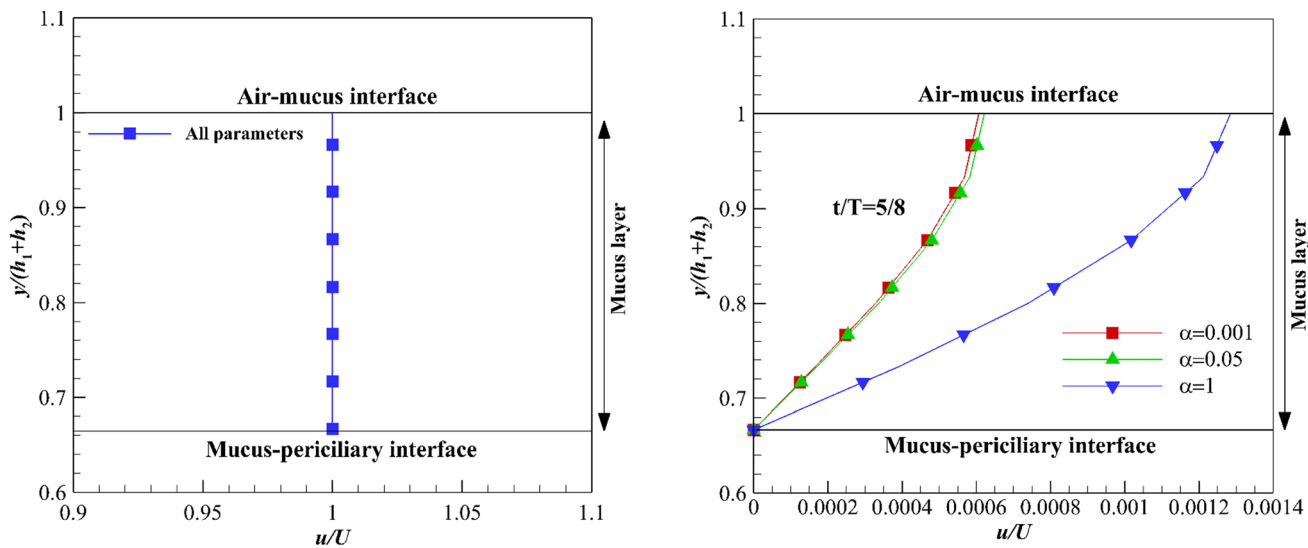

Fig. 13 Velocity variations of the mucus layer using profile (a) along with zero shear stress on the upper bound of the mucus layer for different recovery, breakdown, and breakdown exponent parameters
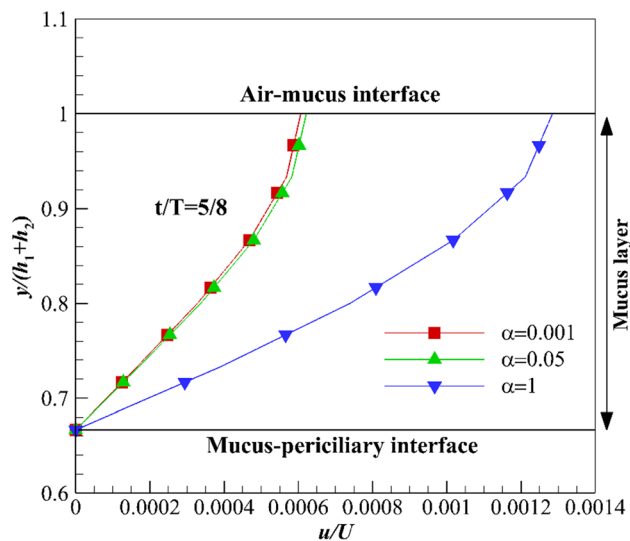
Fig. 14 Velocity variations of the mucus layer using profile (b) in the recovery stroke along with zero shear stress on the upper bound of the mucus layer for different recovery parameters with $\beta_1 = 0.05$ and $\beta_2 = 0.05$

$(t/T = 1/8$ to $t/T = 2/8)$ and $(t/T = 2/8$ to $t/T = 3/8)$ periods, respectively. Therefore, at periods $(t/T = 0$ to $t/T = 1/8)$ and $(t/T = 3/8$ to $t/T = 4/8)$ the adaptation rate of the mucus flow is less than $(t/T = 1/8$ to $t/T = 2/8)$ and $(t/T = 2/8$ to $t/T = 3/8)$ periods. The differences between adaptation rates at two times $t/T = 1/8$ and $t/T = 3/8$ relate to the acceleration rate at period $(t/T = 0$ to $t/T = 1/8)$ and the deceleration rate at period $(t/T = 2/8$ to $t/T = 3/8)$, respectively. The acceleration

rate at period $(t/T = 0$ to $t/T = 1/8)$ is more than the deceleration rate at period $(t/T = 2/8$ to $t/T = 3/8)$. Therefore, mucus flow adapts faster with the changes from the bottom plate at period $(t/T = 2/8$ to $t/T = 3/8)$ than the periods $(t/T = 0$ to $t/T = 1/8)$.

By imposing a complete pattern of cilia motion (profile (d)) at the bottom plate, the obtained results for the effective stroke are the same as those obtained using profile (c),
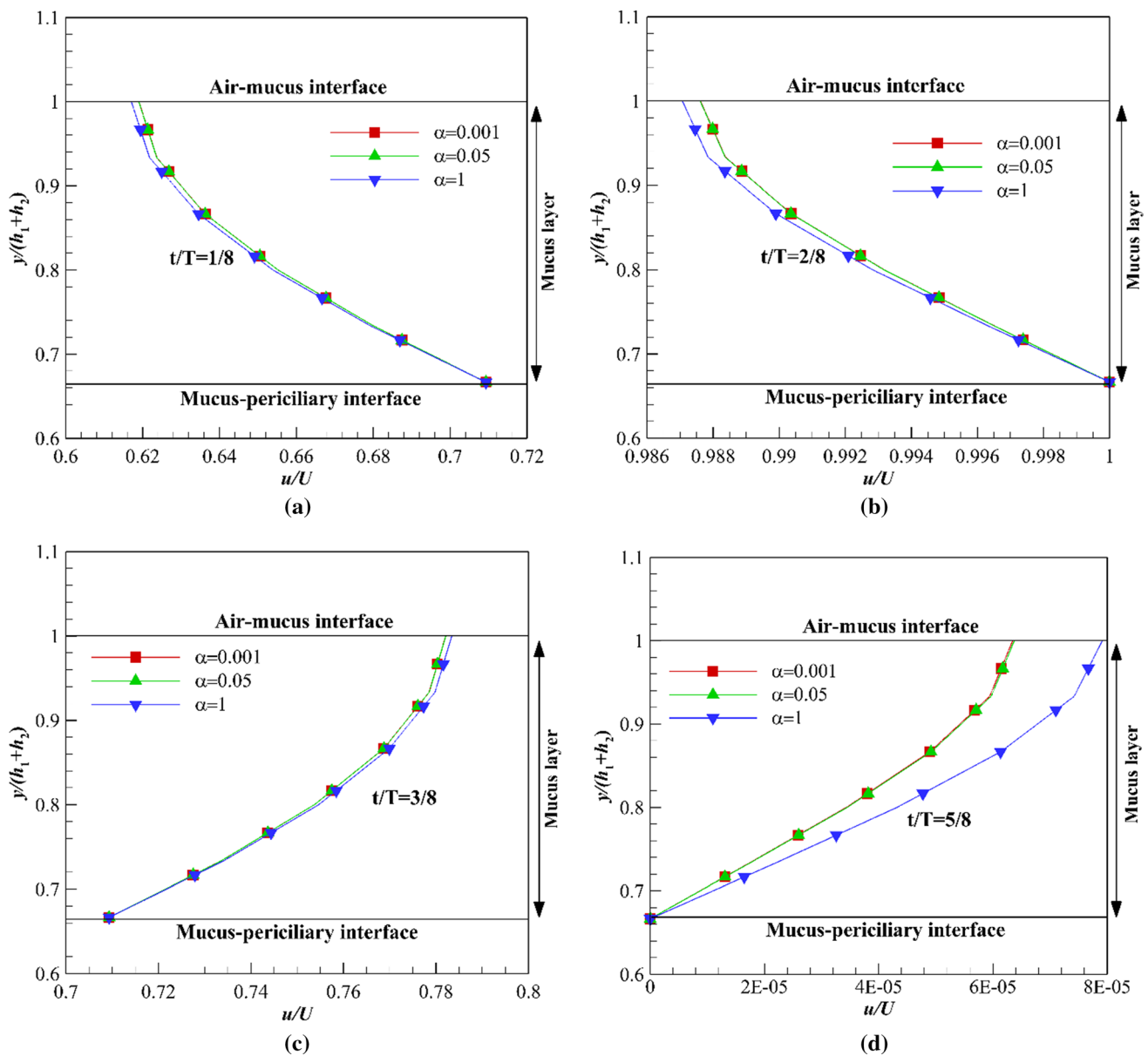
Fig. 15 Velocity variations of the mucus layer using profiles (c) and (d) affected by zero shear stress on the upper bound of the mucus layer for different recovery parameters with $\beta_1 = 0.05$ and $\beta_2 = 0.05$ **a** $t/T = 1/8$, **b** $t/T = 2/8$, **c** $t/T = 3/8$, **d** $t/T = 5/8$ (recovery stroke of profile (d))

Table 3 Maximum adaptation rates for a range of recovery parameters using profile (c)

Times	Maximum adaptation rates for a range of recovery parameters ($\alpha = 10^{-3} - 1$) (%)
$t/T = 1/8$	87
$t/T = 2/8$	99
$t/T = 3/8$	90

because the mucus flow ceases completely in the recovery stroke. The results of recovery stroke are similar to those obtained using profile (b); however, the adaptation rate and the order of velocities are more and lower than the values using profile (b), respectively (Fig. 9), because the mucus flow enters the recovery stroke with the velocity close to zero.
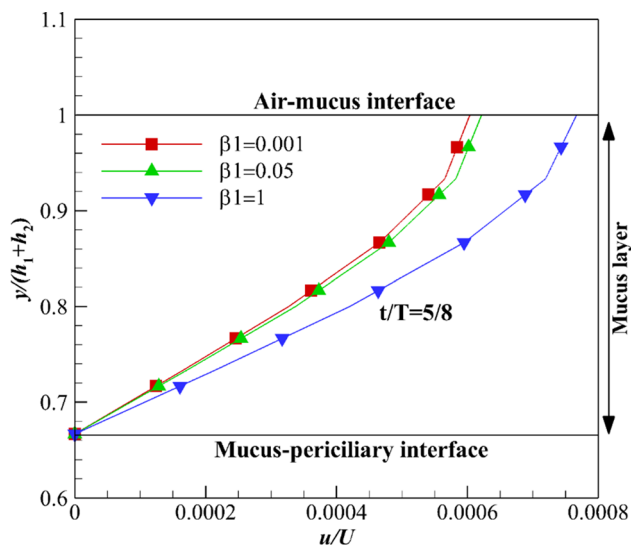
Fig. 16 Velocity variations of the mucus layer using profile (b) in the recovery stroke along with zero shear stress on the upper bound of the mucus layer for different breakdown parameters with $\alpha = 0.05$ and $\beta_2 = 0.05$

6.1.2 Influence of the power index (*n*)

The independence of the mucus layer variations from changes in power index is shown in Figs. 10 and 11. Although different boundary conditions (profiles (a)–(d)) are imposed at the bottom plate, there are no changes in the velocity field using different power indexes. It is concluded that the mucus velocity is independent of the indexes variations and has enough time to adjust the changes from the bottom plate, while $k \geq 0.01$ and $0.2 \leq n < 1$. Figures 10 and 11d show the mucus velocity under the influence of recovery stroke using profiles (b) and (d), respectively. The lower order of velocity filed in the recovery stroke using profile (d) is related to the velocity close to zero at the end of the effective stroke. The same variation of the mucus velocity in the effective stroke using both profiles (c) and (d) is presented in Fig. 11a–c, and the maximum adaptation rates are given in Table 2.

Similar to Table 1, the differences in adaptation rates are due to differences in the acceleration and deceleration rates at different times. According to the results presented in Figs. 5, 6, 7, 8, 9, 10 and 11 and Tables 1 and 2, changes in power law fluid indexes were ineffective on the mucus velocity field. Figure 12a and b shows comparisons between high viscous Newtonian (12 Pa s) and power law fluids for the mucus layer in the effective and recovery strokes that there are no differences between the fluids. Therefore, the power law mucus could be substituted with a high viscous (12 Pa s) Newtonian mucus (Shang et al. 2019; Puchelle et al. 1987).

6.2 Thixotropic mucus layer

To investigate the effects of time-varying viscosity, power law fluid is replaced with thixotropic fluid. In the present study, Burgos's thixotropic model is used as the mucus fluid and the effects of different parameters including recovery, breakdown, and breakdown exponent parameters are evaluated, separately. The evaluation ranges for recovery, breakdown, and breakdown exponent parameters are $(10^{-3} - 1)$, $(10^{-3} - 1)$, and $(5 \times 10^{-4} - 1)$, respectively.

Figure 13 shows the mucus velocity field affected by profile (a) and effective stroke of profile (b) for all fluid parameters in the aforementioned ranges. Although all flow parameters have changed, the effect of boundary conditions is such that the fluid has ample opportunity to adapt to the bottom plate changes. Therefore, uniform distribution is observed all over the mucus layer.

6.2.1 Influence of the recovery parameter (*α*)

The effects of different recovery parameters ($\alpha = 10^{-3} - 1$) in the presence of $\beta_1 = 0.05$ and $\beta_2 = 0.05$ are indicated in Fig. 14 for the recovery stroke. For small recovery parameters, the structural parameter (λ) is small and the effect of the breakdown parameter ($\beta_1 = 0.05$) is greater, i.e., the structure of the fluid is broken. When the fluid microstructure is broken, the behavior of the flow tends to low viscous liquid flow. However, when $\alpha \rightarrow 1$, λ increases, and the effect of the breakdown parameter decreases, thus the structure of the flow is recovered. Increasing the recovery parameter leads to an increase in the recovery rate of the fluid structure, and the mucus flow tends to a solid state. Therefore, with the decline of α the rate of adaptation increases, and the mucus adjusts to the changes from the bottom plate faster.

Regardless of α values, the mucus flow has stopped completely in the recovery stroke and it does not affect the mucus flow pattern in the effective stroke. Therefore, the results using profile (c) and the effective part of profile (d) are the same. Figure 15 shows the variation of mucus flow in the effective stroke for different values of α over time. By increasing time, the rate of adaptation due to the effects of acceleration and deceleration rates over time increases and decreases, repeatedly. As a result, the effects of the recovery parameter on the mucus velocity field are negligible against the rates of acceleration and deceleration over time for the effective stroke (see the previous section). The rates of acceleration and deceleration are related to the frequency and amplitude of the profiles (c) and (d). However, when the bottom plate encounters zero velocity in the recovery stroke
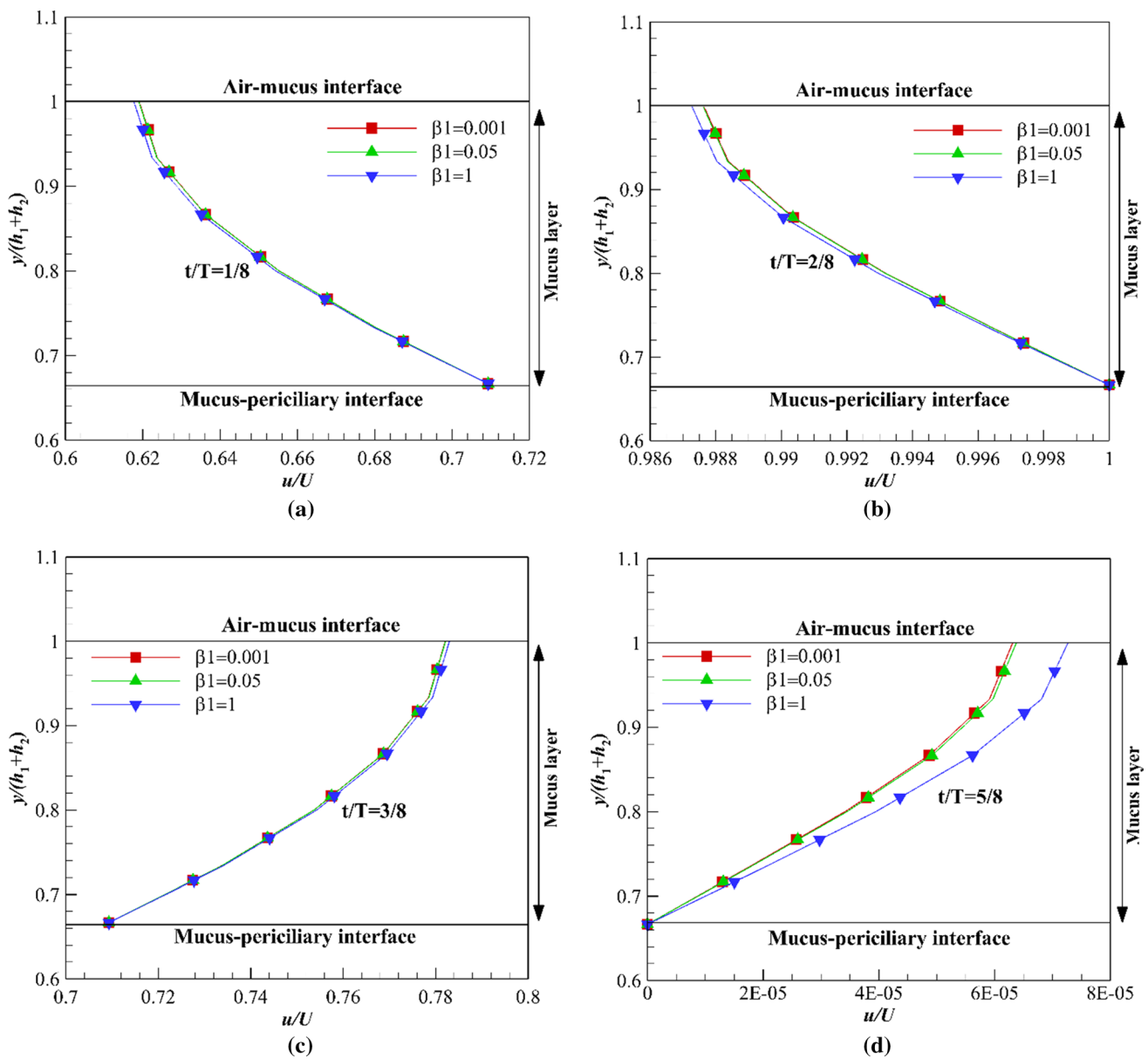
Fig. 17 Velocity variations of the mucus layer using profiles (c) and (d) affected by zero shear stress on the upper bound of the mucus layer for different breakdown parameters with $\alpha = 0.05$ and $\beta_2 = 0.05$ **a** $t/T = 1/8$, **b** $t/T = 2/8$, **c** $t/T = 3/8$, **d** $t/T = 5/8$ (recovery stroke of profile (d))

Table 4 Maximum adaptation rates for a range of breakdown parameters using profile (c)

Times	Maximum adaptation rates for a range of breakdown parameters ($\beta_1 = 10^{-3} - 1$) (%)
$t/T = 1/8$	87.3
$t/T = 2/8$	98.75
$t/T = 3/8$	90.1

(there are no acceleration and deceleration rates), the effects of the recovery parameter become more visible on the mucus flow. The maximum adaptation rates for different recovery parameters are given in Table 3.

6.2.2 Influence of the breakdown parameter (β_1)

Investigation of breakdown parameter ($\beta_1 = 10^{-3} - 1$) on the mucus flow in the presence of $\alpha = 0.05$ and $\beta_2 = 0.05$ is shown in Figs. 16 and 17. Figure 16 is related to the mucus velocity variations in the recovery stroke by increasing the breakdown parameter. According to Fig. 16, increasing the
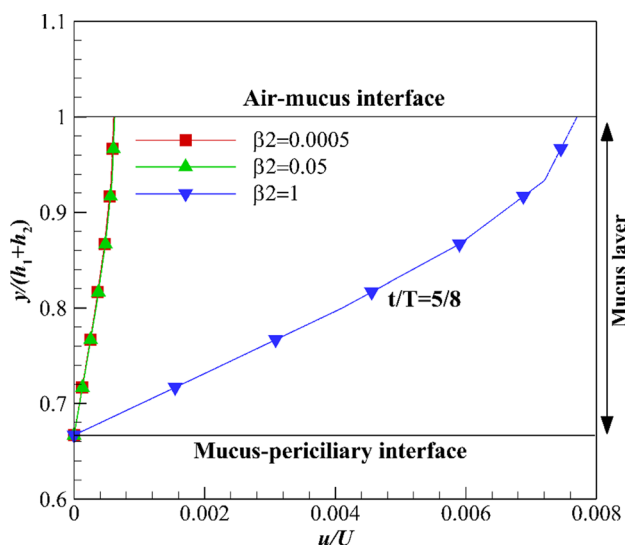
Fig. 18 Velocity variations of the mucus layer using profile (b) in the recovery stroke along with zero shear stress on the upper bound of the mucus layer for different breakdown exponent parameters with $\alpha = 0.05$ and $\beta_1 = 0.05$

breakdown parameter causes the mucus flow to react slower to the changes from the bottom plate. Increasing breakdown parameter causes the reduction of fluid structural parameter, and fluid behaves as a low viscous liquid. In the recovery stroke in which the mucus flow completely ceases, the adaptation rate increases as the β_1 parameter decreases.

Variation of mucus velocity field over time is shown in Fig. 17 for the effective stroke. During the effective stroke, by increasing β_1 parameter the fluid structure is broken more than it recovered, and adjust the changes slowly. Similar to α parameter, the effects of β_1 parameter are negligible against the acceleration and deceleration rates. The reduction of acceleration rate at period ($t/T = 1/8$ to $t/T = 2/8$) against ($t/T = 0$ to $t/T = 1/8$) period causes the mucus flow to obtain sufficient time to adapt to the variations over time (Fig. 17a and b). Thus, the effects of β_1 parameter are small at period ($t/T = 1/8$ to $t/T = 2/8$) and then become significant at $t/T = 3/8$ and $t/T = 5/8$ due to deceleration rate (Fig. 17c and d). Table 4 shows the adaptation rates over time which are taken into account using Eq. 8.

6.2.3 Influence of the breakdown exponent parameter (β_2)

The influence of the breakdown exponent parameter (β_2) is similar to the breakdown parameter (β_1), except that it is more effective on the mucus flow. Figures 18 and 19 show the mucus flow under the influence of β_2 variations. The evaluation range for β_2 is ($5 \times 10^{-4} - 1$) with $\alpha = 0.05$ and $\beta_1 = 0.05$. The effects of β_2 become important, while the value of the recovery parameter is more than β_1 parameter.

In this section due to the equal values for α and β_1 parameters, the role of β_2 parameter is clear. Figure 18 illustrates the variation of velocity for different β_2 parameters in the recovery stroke which adapts to the bottom plate changes slower when $\beta_2 \rightarrow 1$.

The effects of β_2 parameter on the velocity field over time are shown in Fig. 19. Similar to the previous section, by increasing β_2 the mucus flow adjusts to the changes slowly, but the rate of adaptation is different over time. By tending to the maximum velocity, the effect of β_2 decreases due to the reduction of acceleration rate and increases in the deceleration rates (Fig. 19a–d). The maximum rates of adaptation are given in Table 5 for different β_2 parameters over time.

Inspection of the velocity field using three different recovery, breakdown, and breakdown exponent parameters shows the mucus flow variations are independent of all values of α, β_1, β_2 in the effective stroke. However, independence of the mucus flow variations occurs for α, β_1, $\beta_2 \leq 0.05$ in the recovery stroke. To examine the replacement of the thixotropic fluid with a high viscous Newtonian fluid, variations of the mucus velocity for different fluid parameters are investigated (Fig. 20a and b). The maximum difference between Newtonian and thixotropic fluids is 1% for the effective stroke, while it is more than 98.5% for the recovery stroke. Differences are calculated using Eq. (9).

$$\frac{\left| \left(\frac{u}{U} \right)_{\text{Newtonian}} - \left(\frac{u}{U} \right)_{\text{Thixotropic}} \right|}{\left(\frac{u}{U} \right)_{\text{Thixotropic}}} \times 100 \tag{9}$$

Based on the results obtained for the velocity field, it is concluded that the replacement of thixotropic fluid with Newtonian fluid is only acceptable in the effective stroke. However, the difference between results is so great in the recovery stroke that the replacement of the thixotropic fluid with a Newtonian fluid is invalid. The velocity using thixotropic fluid (7×10^{-5}) is at least two orders of magnitude higher than Newtonian fluid (10^{-6}).

7 Concluding remarks

The velocity variations of the mucus layer were evaluated using power law and thixotropic fluids under different cyclic boundary conditions. The effects of changes in the fluid model parameters were examined on the mucus velocity field. The results showed differences were negligible due to replacing the power law fluid with the Newtonian fluid. Therefore, replacing the power law fluid with the Newtonian fluid was acceptable when zero shear stress was applied on the upper bound of the mucus layer. However,
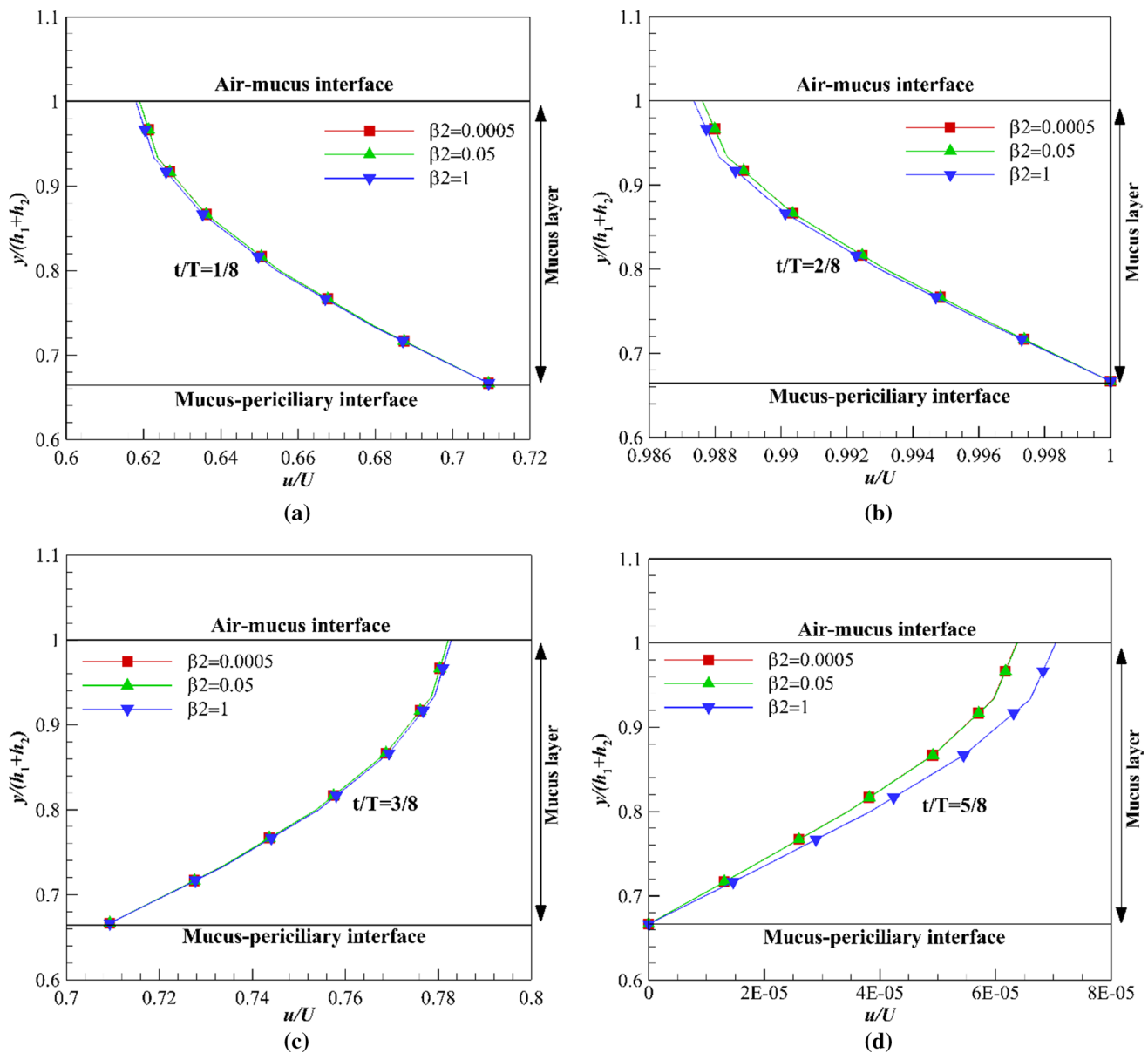
Fig. 19 Velocity variations of the mucus layer using profiles (c) and (d) affected by zero shear stress on the upper bound of the mucus layer for different breakdown exponent parameters with $\alpha = 0.05$ and $\beta_1 = 0.05$ **a** $t/T = 1/8$, **b** $t/T = 2/8$, **c** $t/T = 3/8$, **d** $t/T = 5/8$ (recovery stroke of profile (d))

Table 5 Maximum adaptation rates for a range of breakdown exponent parameters using profile (c)

Times	Maximum adaptation rates for a range of breakdown exponent parameters ($\beta_2 = 5 \times 10^{-4} - 1$) (%)
$t/T = 1/8$	87
$t/T = 2/8$	98.8
$t/T = 3/8$	89.7

the substitution of thixotropic fluid with the Newtonian fluid was acceptable only for the effective stroke (maximum difference value was 1%), because both fluids have a high order of differences (98.5%) in the recovery stroke. On the other hand, the rates of adaptation indicated the mucus flow had ample opportunity to adapt to the changes resulting from the bottom plate. Thus, the mucus flow ceased completely in the recovery stroke and it did not affect the velocity field in the effective stroke. The maximum adaptation rate was
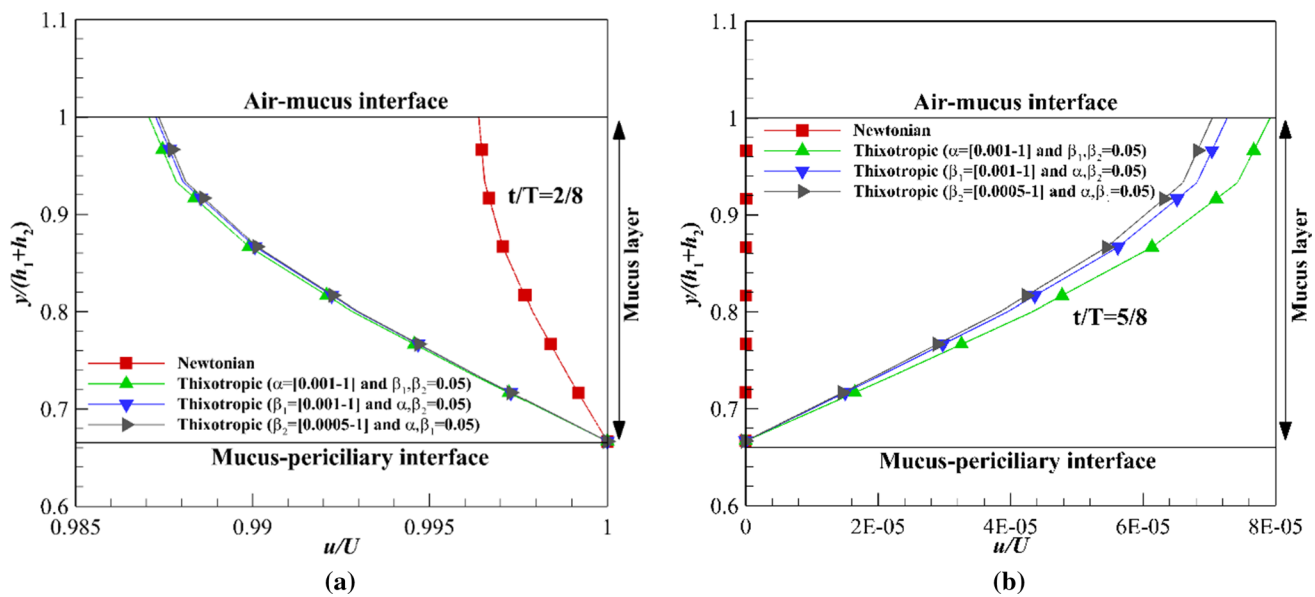
Fig. 20 Comparison of mucus layer velocity using both Newtonian and thixotropic fluids affected by profile (d) and zero shear stress on the upper bound of the mucus layer for different recovery, breakdown, and breakdown exponent parameters **a** effective stroke, **b** recovery stroke

taken into account for each case, and it was concluded the rate of acceleration and deceleration had significant effects on the adaptation rate. It was observed that the effects of recovery, breakdown, and breakdown exponent parameters on the mucus flow variations were the same for the effective stroke and led to similar adaptation rates. However, velocity variations showed the effects of the exponent parameter were more than the other two parameters in the recovery stroke. In the continuation of the present work, the viscoelastic effects can be studied using the 5-mode nonlinear Giesekus model. Moreover, the effects of movement induced by the separation of cilia from the mucus layer in the recovery stroke can be investigated, because in the current study the recovery stroke is zero, while in the real model it is opposite to zero. It is also better to use real cilia motion in connection with the mucus layer than a movement plate to obtain more accurate information about the mucus flow in the nasal airway system.

References

Barton C, Raynor S (1967) Analytical investigation of cilia induced mucous flow. Bull Math Biophys 29(3):419–428

Blake JR (1971) A spherical envelope approach to ciliary propulsion. J Fluid Mech 46(1):199–208

Blake J (1972) A model for the micro-structure in ciliated organisms. J Fluid Mech 55(1):1–23

Blake J (1975) On the movement of mucus in the lung. J Biomech 8(3–4):179–190

Brennen C (1974) An oscillating-boundary-layer theory for ciliary propulsion. J Fluid Mech 65(4):799–824

Brennen C, Winet H (1977) Fluid mechanics of propulsion by cilia and flagella. Annu Rev Fluid Mech 9(1):339–398

Bui CM, Ho TX (2020) Influence of thixotropic parameters on a non-Newtonian fluid flow. AIP Adv 10(3):035303

Burgos GR, Alexandrou AN, Entov V (2001) Thixotropic rheology of semisolid metal suspensions. J Mater Process Technol 110(2):164–176

Celik IB, Ghia U, Roache PJ (2008) Procedure for estimation and reporting of uncertainty due to discretization in {CFD} applications. J Fluids (Eng-Trans ASME) **130**(7).

Chatelin R, Poncet P (2016) A parametric study of mucociliary transport by numerical simulations of 3D non-homogeneous mucus. J Biomech 49(9):1772–1780

Chatelin R et al (2017) Numerical and experimental investigation of mucociliary clearance breakdown in cystic fibrosis. J Biomech 53:56–63

Chen X et al (2018) Effects of thermal airflow and mucus-layer interaction on hygroscopic droplet deposition in a simple mouth–throat model. Aerosol Sci Technol 52(8):900–912

Chowdhury MA et al (2020) Immune response in COVID-19: A review. J Infection and Public Health**.

Corbo G et al (1989) Measurement of nasal mucociliary clearance. Arch Dis Child 64(4):546–550

Cornaz A-L, Buri P (1994) Nasal mucosa as an absorption barrier. Eur J Pharm Biopharm 40(5):261–270

Cortez R, Fauci L, Medovikov A (2005) The method of regularized Stokeslets in three dimensions: analysis, validation, and application to helical swimming. Phys Fluids 17(3):031504

Dalhamn T (1956) Mucous flow and ciliary activity in the trachea of healthy rats and rats exposed to respiratory irritant gases (SO2, H3N, HCHO): a functional and morphologic (light microscopic and electron microscopic) study, with special reference to technique. Acta Physiol Scand Suppl 36(123):1

Derichs N et al (2011) Hyperviscous airway periciliary and mucous liquid layers in cystic fibrosis measured by confocal fluorescence photobleaching. FASEB J 25(7):2325–2332

Dillon RH et al (2007) Fluid dynamic models of flagellar and ciliary beating. Ann N Y Acad Sci 1101(1):494–505

Dusenbery DB (2009) Living at micro scale: the unexpected physics of being small. Harvard University Press, Harvard.

Eloy C, Lauga E (2012) Kinematics of the most efficient cilium. Phys Rev Lett 109(3):038101

Farrell PM (2008) The prevalence of cystic fibrosis in the European Union. J Cyst Fibros 7(5):450–453

Fauci LJ, Dillon R (2006) Biofluidmechanics of reproduction. Annu Rev Fluid Mech 38:371–394

Flórez-Orrego D et al (2012) Experimental and CFD study of a single phase cone-shaped helical coiled heat exchanger: an empirical correlation. In: Proceedings of the 25th International Conference on Efficiency, Cost, Optimization, Simulation and Environmental Impact of Energy Systems

Gizurarson S (2015) The effect of cilia and the mucociliary clearance on successful drug delivery. Biol Pharmaceutical Bull, p. b14-00398.

Gray J (1939) The kinetics of locomotion of Nereis diversicolor. J Exp Biol 23:101–120

Gray J, Hancock G (1955) The propulsion of sea-urchin spermatozoa. J Exp Biol 32(4):802–814

Gsell S et al (2020) Hydrodynamic model of directional ciliary-beat organization in human airways. Sci Rep 10(1):1–12

Gueron S, Liron N (1992) Ciliary motion modeling, and dynamic multicilia interactions. Biophys J 63(4):1045–1058

Guo H et al (2017) Bistability in the synchronization of actuated microfilaments. arXiv preprint arXiv:1708.02181.

Hollenberg M (1986) Mechanisms of receptor-mediated transmembrane signalling. Experientia 42(7):718–727

Illum L (2003) Nasal drug delivery—possibilities, problems and solutions. J Control Release 87(1–3):187–198

Ishtiaq F et al (2022) Insight in thermally radiative cilia-driven flow of electrically conducting non-newtonian jeffrey fluid under the influence of induced magnetic field. Mathematics 10(12):2007

Javid K et al (2021) Cilia-assisted flow of viscoelastic fluid in a divergent channel under porosity effects. Biomech Model Mechanobiol 20(4):1399–1412

Kahramanoglu E, Sezen S, Bayraktar S (2017) Computational fluid dynamics analyses on the hydrodynamic entry length in internal flows. Pamukkale Univ J Eng Sci 23(4).

Khashkhosha HK, Elhadi M (2020) A hypothesis on the role of the human immune system in covid-19. Med Hypotheses 143:110066

King M, Agarwal M, Shukla J (1993) A planar model for mucociliary transport: effect of mucus viscoelasticity. Biorheology 30(1):49–61

Lai SK et al (2009) Micro-and macrorheology of mucus. Adv Drug Deliv Rev 61(2):86–100

Lale A, Mason J, Jones N (1998) Mucociliary transport and its assessment: a review. Clin Otolaryngol Allied Sci 23(5):388–396

Lauga E, Powers TR (2009) The hydrodynamics of swimming microorganisms. Rep Prog Phys 72(9):096601

Lee W et al (2011) Muco-ciliary transport: effect of mucus viscosity, cilia beat frequency and cilia density. Comput Fluids 49(1):214–221

Lubkin D, Gaffney E, Blake J (2007) A viscoelastic traction layer model of muco-ciliary transport. Bull Math Biol 69(1):289

Matar O, Craster R, Warner M (2002) Surfactant transport on highly viscous surface films. J Fluid Mech 466:85

Matthews LW et al (1963) Studies on pulmonary secretions: I. The over-all chemical composition of pulmonary secretions from patients with cystic fibrosis, bronchiectasis, and laryngectomy. Am Rev Respiratory Dis 88(2):199–204.

Mistry A, Stolnik S, Illum L (2009) Nanoparticles for direct nose-to-brain delivery of drugs. Int J Pharm 379(1):146–157

Mitran SM (2007) Metachronal wave formation in a model of pulmonary cilia. Comput Struct 85(11–14):763–774

Myon L et al (2010) Palatal necrosis due to cocaine abuse. Rev Stomatol Chir Maxillofac 111(1):32

Osterman N, Vilfan A (2011) Finding the ciliary beating pattern with optimal efficiency. Proc Natl Acad Sci 108(38):15727–15732

Pires A et al (2009) Intranasal drug delivery: how, why and what for? J Pharm Pharm Sci 12(3):288–311

Potter JL et al (1967) Studies on pulmonary secretions: II. Osmolality and the ionic environment of pulmonary secretions from patients with cystic fibrosis, bronchiectasis, and laryngectomy. Am Rev Respiratory Dis 96(1):83–87.

Puchelle E, Zahm J, Quemada D (1987) Rheological properties controlling mucociliary frequency and respiratory mucus transport. Biorheology 24(6):557–563

Quraishi M, Jones N, Mason J (1998) The rheology of nasal mucus: a review. Clin Otolaryngol Allied Sci 23(5):403–413

Roohi E, Pendar M-R, Rahimi A (2016) Simulation of three-dimensional cavitation behind a disk using various turbulence and mass transfer models. Appl Math Model 40(1):542–564

Ross S, Corrsin S (1974) Results of an analytical model of mucociliary pumping. J Appl Physiol 37(3):333–340

Round G (1980) An explicit approximation for the friction factor-Reynolds number relation for rough and smooth pipes. Can J Chem Eng 58(1):122–123

Rusznak C et al (1994) The assessment of nasal mucociliary clearance and the effect of drugs. Respir Med 88(2):89–101

Sanderson MJ, Sleigh MA (1981) Ciliary activity of cultured rabbit tracheal epithelium: beat pattern and metachrony. J Cell Sci 47(1):331–347

Satir P, Sleigh MA (1990) The physiology of cilia and mucociliary interactions. Annu Rev Physiol 52(1):137–155

Schneiter M et al (2021) Multi-scale alignment of respiratory cilia and its relation to mucociliary function. J Struct Biol 213(1):107680

Sedaghat M et al (2016a) Effect of cilia beat frequency on muco-ciliary clearance. J Biomed Phys Eng 6(4):265

Sedaghat M et al (2016b) On the effect of mucus rheology on the muco-ciliary transport. Math Biosci 272:44–53

Shang Y, Inthavong K, Tu J (2019) Development of a computational fluid dynamics model for mucociliary clearance in the nasal cavity. J Biomech 85:74–83

Singh PK et al (2002) A component of innate immunity prevents bacterial biofilm development. Nature 417(6888):552–555

Sleigh M (1977) The nature and action of respiratory tract cilia. Respiratory Defense Mechanisms Part 1:247–288

Smith D, Gaffney E, Blake J (2008) Modelling mucociliary clearance. Respir Physiol Neurobiol 163(1–3):178–188

Snyder SH, Sklar PB, Pevsner JA (1988) Molecular mechanisms of olfaction. J Biol Chem 263(28):13971–13974

Sundararaman A et al (2020) Role of probiotics to combat viral infections with emphasis on COVID-19. Appl Microbiol Biotechnol, pp 1–16.

Ugwoke MI, Verbeke N, Kinget R (2001) The biopharmaceutical aspects of nasal mucoadhesive drug delivery. J Pharm Pharmacol 53(1):3–22

Vasquez PA et al (2016) Modeling and simulation of mucus flow in human bronchial epithelial cell cultures–Part I: Idealized axisymmetric swirling flow. PLoS Comput Biol 12(8):e1004872

Xu L, Jiang Y (2019) Mathematical modeling of mucociliary clearance: a mini-review. Cells 8(7):736

Zanin M et al (2016) The interaction between respiratory pathogens and mucus. Cell Host Microbe 19(2):159–168

Zhu P-F et al (2019) Simulation Study on the Mass Transport Based on the Ciliated Dynamic System of the Respiratory Tract. Comput Math Methods Med.

Publisher's Note Springer Nature remains neutral with regard to jurisdictional claims in published maps and institutional affiliations.